Physics Letters B 809 (2020) 135739

Contents lists available at ScienceDirect

Physics Letters B

www.elsevier.com/locate/physletb

7-order enhancement of the Stern-Gerlach effect of neutrons diffracting in a crystal

V.V. Voronin [a,b,c,*], S.Yu. Semenikhin [a,b], D.D. Shapiro [a,c], Yu.P. Braginets [a,b], V.V. Fedorov [a,b,c], V.V. Nesvizhevsky [d], M. Jentschel [d], A. Ioffe [e], Ya.A. Berdnikov [b]

[a] Petersburg Nuclear Physics Institute named by B.P. Konstantinov of NRC "Kurchatov Institute", 188300, Gatchina, Russia
[b] Peter the Great St. Petersburg Polytechnic University, 195251, Saint Petersburg, Russia
[c] St Petersburg University, 199034, Saint Petersburg, Russia
[d] Institut Laue-Langevin, 38042 Grenoble, France
[e] Jülich Centre for Neutron Science JCNS, Forschungszentrum Jülich GmbH, MLZ, 85747 Garching, Germany

ARTICLE INFO

Article history:
Received 30 April 2020
Received in revised form 17 August 2020
Accepted 25 August 2020
Available online 27 August 2020
Editor: D.F. Geesaman

Keywords:
Neutron
Single crystal
Stern-Gerlach effect
Dynamic diffraction
Magnetic field
Equivalence principle

ABSTRACT

We measured the spatial splitting of a non-polarized neutron beam passed through a crystal under diffraction conditions in heterogeneous magnetic field (analog to the Stern-Gerlach effect) into two polarized components with opposite polarization. The measurements were carried out using Laue diffraction scheme, small gradients of the magnetic field and Bragg angles close to orthogonality $\theta_B = (78 - 82)°$. After a flight path in crystal of 21.6 cm a splitting of 4.1 ± 0.1 cm was achieved (using a field gradient of ~ 3 G/cm and a diffraction angle of 82°). In the absence of a diffraction (crystal) but otherwise the same flight path and field gradient the spatial splitting would be $\sim 4 \cdot 10^{-7}$ cm. From those we deduce an experimental amplification factor in the order of about $\sim 2 \cdot 10^5 \tan^2 \theta_B$ due to the use of diffraction in crystals, which agrees with theory.

1. Introduction

In the frame work of preparation towards a larger experiment to probe the weak equivalence principle for neutrons [1] we carried out a measurement to investigate the diffractive amplification of small interactions of the neutron. This can be achieved by using Laue diffraction in crystals with Bragg angles close to 90°. The spatial splitting of an unpolarized neutron beam due to the presence of a magnetic field gradient (~ 3 G/cm) into two polarized beams with opposite spin orientation (analog to Stern-Gerlach effect) was amplified via Laue diffraction on a crystal and measured.

2. Theory

According to the dynamic theory of diffraction [2] neutron propagation in a crystal in nearly Bragg directions for a certain system of crystallographic planes can be described by two types of Bloch waves $\psi^{(1)}$ and $\psi^{(2)}$. They are formed because of the interaction of the neutron with a periodic nuclear potential of this system of crystallographic planes, which is characterized by the reciprocal lattice vector g that is perpendicular to the planes and has the length $|\mathbf{g}| \equiv g = 2\pi/d$, where d is the interplanar distance. The corresponding harmonic of the periodic nuclear potential has the form

$$V_g(\mathbf{r}) = 2V_g \cos \mathbf{gr}. \tag{1}$$

The amplitude of the harmonic is determined by the structural amplitude of the nuclear scattering of the neutron by a crystal cell:

$$V_g^N = \frac{2\pi\hbar^2}{m} N_c F_g^N,$$
$$F_g^N = \sum_i \exp(-W_{ig}) f_i^N(\mathbf{g}) \exp(i\mathbf{gr}_i). \tag{2}$$

Here, m is the neutron mass, N_c is the number of unit cells in unit volume of the crystal, the subscript i specifies atoms in a unit cell, $\mathbf{r}_i$ is the position of the nucleus of the ith atom in the unit cell, $f_i^N(\mathbf{g})$ is the scattering amplitude by the ith nucleus of the unit cell with the momentum transfer $\mathbf{g}$, and W_{ig} is the Debye-Waller factor. Note that the structural forward scattering amplitude ($\mathbf{g} = 0$) determines the average nuclear potential of the crystal (and, thereby, its average refractive index).

* Corresponding author.
E-mail address: voronin_vv@pnpi.nrcki.ru (V.V. Voronin).

https://doi.org/10.1016/j.physletb.2020.135739

The waves $\psi^{(1)}$ and $\psi^{(2)}$ are two orthogonal superpositions of the direct wave with the wavevector $\mathbf{k}$ and the wave with the wavevector $\mathbf{k}+\mathbf{g}$ reflected from crystallographic planes:

$$\psi^{(1)}(\mathbf{r}) = \cos\gamma e^{i\mathbf{k}^{(1)}\mathbf{r}} + \sin\gamma e^{i[\mathbf{k}^{(1)}+\mathbf{g}]\mathbf{r}}, \tag{3}$$

$$\psi^{(2)}(\mathbf{r}) = -\sin\gamma e^{i\mathbf{k}^{(2)}\mathbf{r}} + \cos\gamma e^{i[\mathbf{k}^{(2)}+\mathbf{g}]\mathbf{r}}. \tag{4}$$

Here

$$\tan 2\gamma = \frac{U_g^N}{\Delta_g} \equiv \frac{1}{w_g}, \tag{5}$$

where

$$U_g^N = \frac{2mV_g^N}{\hbar^2} \tag{6}$$

and

$$\Delta_g = \frac{(\mathbf{k}+\mathbf{g})^2 - k^2}{2} = \frac{2\mathbf{kg}+g^2}{2}. \tag{7}$$

The dimensional (Δ_g) and dimensionless (w_g) parameters describe a deviation from the Bragg condition.

The wavevectors $\mathbf{k}^{(1)}$ and $\mathbf{k}^{(2)}$ belong to different branches of the dispersion surface, which is specified by the equation

$$\left(\mathbf{k}^{(1,2)}\right)^2 = K^2 - \Delta_g \mp \sqrt{\Delta_g^2 + \left(U_g^N\right)^2}. \tag{8}$$

Here, $K^2 = k_e^2(1 - V_0^N)$ is the length squared of the wavevector of the neutron incident on the crystal taking into account the average refractive index of the crystal, where k_e is the wavevector of the neutron in vacuum. For $\cos^2\gamma$ in Eqs. (3) and (4), we have

$$\cos^2\gamma = \frac{1}{2}\left[1 + \frac{\Delta_g}{\sqrt{\Delta_g^2 + \left(U_g^N\right)^2}}\right] = \frac{1}{2}\left[1 + \frac{w_g}{\sqrt{1+w_g^2}}\right]. \tag{9}$$

Under the exact Bragg condition ($w_g = 0$), $\psi^{(1)}$ and $\psi^{(2)}$ are the symmetric and antisymmetric combinations of the direct and reflected waves, respectively. They propagate along crystallographic planes (in the direction $\mathbf{k}_{||} = \mathbf{k} + \mathbf{g}/2$, see Fig. 1) with the velocity $v_{||} = v\cos\theta_B$. Neutrons in the states $\psi^{(1)}$ and $\psi^{(2)}$ are concentrated predominantly in and between nuclear planes, respectively ("nuclear" planes are determined by the maxima of the nuclear potential). Consequently, neutrons in the states $\psi^{(1)}$ and $\psi^{(2)}$ move in different potentials and have slightly different kinetic energies (i.e., different wavevectors) and different absorption. Deviation from the Bragg condition leads to changes in current density directions and toward opposite sides.

In the case of symmetric Laue diffraction (the input face of the crystal is perpendicular to reflecting planes), boundary conditions for the wave function inside the crystal give [2]

$$\psi(\mathbf{r}) = \psi^{(1)}(\mathbf{r})\cos\gamma + \psi^{(2)}(\mathbf{r})\sin\gamma. \tag{10}$$

Thus, at small deviations from the Bragg condition ($w_g \ll 1$), both states are excited with almost the same probability. However, the directions of the neutron current densities $\mathbf{j}_{\psi^{(1)}}$ and $\mathbf{j}_{\psi^{(2)}}$ in these states can change very significantly when Bragg angles θ_B are close to 90°, i.e., when $k_{||} \ll g/2$ ($\tan\theta_B = g/2k_{||} \gg 1$) (see Fig. 1):

$$\mathbf{j}_{\psi^{(1,2)}} \approx \frac{\hbar}{m}\left[\mathbf{k}_{||}^{(1,2)} \pm \frac{\mathbf{g}}{2}w_g\right]. \tag{11}$$

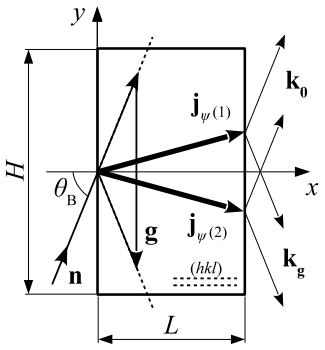

Fig. 1. Symmetric Laue diffraction in an undeformed finite crystal. Neutrons $\mathbf{n}$ are incident on the crystal at a certain angle different from the Bragg angle θ_B within the Bragg (Darwin) width; $\mathbf{j}_{\psi^{(1)}}$ and $\mathbf{j}_{\psi^{(2)}}$ are the neutron flux density vectors of two Bloch waves, $\mathbf{g}$ is the reciprocal lattice vector, L is the crystal thickness and H is the height. Here "Kato trajectories" are straight lines directed along the current density vectors.

3. External force and "Kato trajectories"

The propagation of a neutron (two-wave packet) under action of external force (or in slightly deformed crystal) from a certain region on the input face in a crystal can be described by "Kato trajectories" [3]. They are curves tangents to which are directed along the current density vector at each point of the trajectory. In an undeformed crystal, and when the external force is absent, Kato trajectories are straight lines (see Fig. 1), whose slopes are determined by the parameter w_g. When the direction of the incident beam is varied within the Bragg angular width, the angle of inclination θ of the Kato trajectory will be varying from $-\theta_B$ to $+\theta_B$. At Bragg angles close to the right angle, the dimensions of the crystal (H is the height and L is the thickness) can restrict possible angles of inclination of trajectories if $\tan\theta = H/2L < \tan\theta_B$ as in our case.

An external force, acting on the diffracting neutron inside the crystal can slightly change the direction of motion (and/or its wavelength). This results in a deviation from the Bragg condition and change of the amplitudes of the direct and diffracted waves inside the crystal. As a result, a substantial deviation of the direction of neutron current in the crystal will take place.

In the experiment a double crystal layout as shown in Fig. 2 was used.

A bending of the Kato trajectory due to external force F_w in a double crystal scheme leads to a spatial shift of the neutron beam at the exit face of the second crystal. In order to identify the neutrons deviating from the Bragg condition (Kato trajectory) the neutron flux is collimated by two slits S_1 and S_2 at the first and second crystal. The spatial distribution of the neutron beam at the exit of the second crystal is obtained by a scanning slit S_3.

In Fig. 2 we show by red and blue lines the two Kato trajectories of neutrons with opposite spin projection weakly absorbed inside the crystal (which belong to one of two branches of the neutron dispersion surface in crystal). Having in mind the experimental conditions (large thickness of the crystals and large Bragg angles) the neutrons in other diffracting branches are almost completely absorbed due to the Borman effect [4] by the silicon crystal and the according Kato trajectories disappear.

The effect of diffractive amplification of the deviation of a neutron beam inside a crystal is well known long ago. This is why the diffraction is widely used to study the fundamental properties and interactions of the neutron. Those are the development of new methods for searching for the neutron electric dipole moment [5–12], a search for hypothetical CP-violating forces [13], the study of the neutrons interaction with gravitational and magnetic fields [8,14–16], as well of the effects of neutron acceleration in

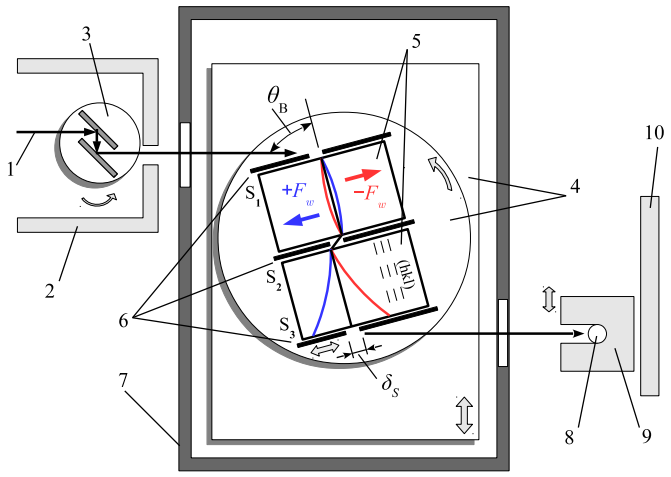

Fig. 2. Double crystal experimental layout (top view): 1 – neutron beam; 2 – concrete hutch; 3 – double-crystal monochromator; 4 – translation stage for the crystals including a rotation stage; 5 – two silicon single crystals; 6 – collimating (S_1, S_2) and scanning (S_3) slits; 7 – thermostat; 8 – detector; 9 – detector shielding; 10 – beam dump.

variable magnetic fields [17,18] and in an accelerating crystal [19]. Also there are interesting studies of the Schwinger (spin-orbit) interaction of the neutron with interplanar electric fields in centrosymmetric [20,21] and non-centrosymmetric crystal [7,9,22–24] in diffraction and also of its application to control neutron polarization at Laue diffraction in the perfect slightly deformed crystal with controlled deformation using a small temperature gradient [25].

The effect of diffractive amplification has been directly measured by Zeilinger et al. [15], with using neutron beam deflection in inhomogeneous magnetic field. The deflection was more 10^5 times (actually $2.1 \cdot 10^5$) larger than in the same fields in free space. The authors [15] have obtained the splitting of non-polarized beam into two also non-polarized beams in contrast to the present work. In this paper, we exploit two additional factors related to the use of large Bragg angles and large crystal sizes.

First, there is another gain associated with large diffraction angles close to 90°, which is proportional to $\tan^2\theta_B$. Its existence is based on the fact that diffraction is not governed by the neutrons total velocity v_n, but its projection onto the crystallographic planes $v_{||} = v_n \cos\theta_B$ [26,27]. When the diffraction angle is increased the time spent by the neutron inside the crystal, is growing proportional to $\tan\theta_B$ [28]. This gives a new additional amplification scheme for measuring forces weakly interacting with the diffracting neutron.

Secondly, for thick crystals and large Bragg angles, due to increasing the time spent by the neutron inside the crystal, effective path of neutron in the crystal increases significantly too, so the effect of abnormal absorption (Borman effect) becomes very pronounced. It was measured [4] for used silicon crystal and results in that only neutrons in the weakly absorbed state survive in contrast to ref. [15]. Therefore, the corresponding Kato trajectory splits only due to two opposite forces acting on neutrons with opposite spin orientations (Fig. 2), so that the spatial separation of the spins occurs, as in the Stern-Gerlach effect, but significantly larger in magnitude.

The present experiment is particularly focusing on demonstrating the extraordinary sensitivity with respect to external forces acting on the neutron inside the crystal. The force F_w, necessary to displace the neutron beam at the exit of the second crystal (in the case of three collimating slits and the equal distance L between them) by a distance equal to the slit width δ_s, is [29]

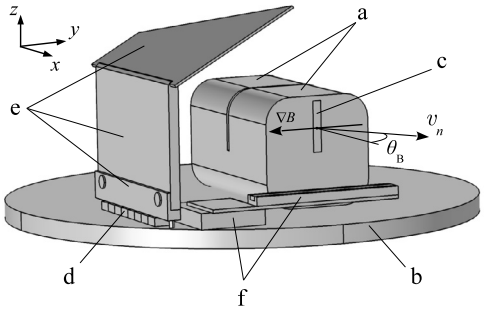

Fig. 3. Schematic view on probing silicon crystal and magnetic field guide: a – probing silicon crystal, b – rotation stage (also part of field guide), c – neutron beam exit area, d – permanent magnets, e – magnetic field guide, f – piezomotor positioner of exit slit S_3 (slit is not shown).

$$F_w = \frac{m_0 d}{\pi \tan^2\theta_B} \cdot \frac{2E_n}{L^2} \cdot \delta_s \equiv \frac{1}{K_e} \cdot \frac{2E_n}{L^2} \cdot \delta_s, \tag{12}$$

where K_e – is the total coefficient of diffractive amplification, $(2E_n\delta_s)/L^2$ – the force, perpendicular to the direction of motion of the neutron and necessary for a displacement of δ_s in vacuum, $m_0 \equiv 2F_g d/V$ – the "Kato mass", V – the crystals unit cell volume, F_g – the neutron scattering structure amplitude for the crystals unit cell, E_n – the neutron energy, L – the thickness of one crystal.

For the (220) planes of silicon with an interplane distance of $d = 1.92$ Å, as used in the present experiment and for $m_0 = 774.4$ cm^{-1}, the diffractive amplification coefficient becomes

$$K_e^{(220)} = \frac{\pi \tan^2\theta_B}{m_0 d} = 2.1 \cdot 10^5 \cdot \tan^2\theta_B \tag{13}$$

which predicts a value of $K_e^{(220)} = 1.1 \cdot 10^7$ for a maximum Bragg angle of 82° in the experiment.

4. The setup

The experiment was carried out in 2018 at the PF1b cold neutron beam facility [30] of the Institut Laue-Langevin, Grenoble, France. A schematic view of the experiment was shown above in Fig. 2. At the beginning the beam of nonpolarized cold neutrons (1) is passing onto the monochromator (3), which is shielded by a concrete hutch (2). The monochromator, apart from selecting a wave length and divergence diapason, is also lowering the neutron flux falling onto the actual silicon crystal (5). This also decreases the ambient background substantially. The monochromator is mounted on a rotation stage and consists of two crystals of pyrolitic graphite (PG) having the (002) planes ($d_{PG} = 3.35$ Å) oriented to the parallel-opposite crystal faces. The reflected wave length can be tuned via the rotation stage within a range of $\lambda = (3.5 - 3.9)$ Å. The mosaicity of the crystals is $\sim 0.9°$, which allows to achieve a monochromaticity of $\Delta\lambda/\lambda \sim 10^{-2}$.

The neutron beam from the monochromator is impinging the entry face of the probing silicon crystal (5) having dimensions of 130 mm × 130 mm × 218 mm. In the experiment the (220) diffraction planes with an interplane spacing of $d = 1.92$ Å were used.

The maximum variation of the interplanar spacing $\Delta d/d$ over the entire crystal volume should be no more than $\sim 10^{-7}$ to observe the effect. Larger gradients of interplanar distance will lead to additional Kato forces, acting in the same directions and with the comparable value as the magnetic gradients, and so to the broadening of the Kato trajectories and the intensity distribution profiles on the output face of the crystal, to a decrease in intensity and the disappearance of the effect. To obtain a double crystal geometry the silicon crystal has a cut with a depth of 72 mm and

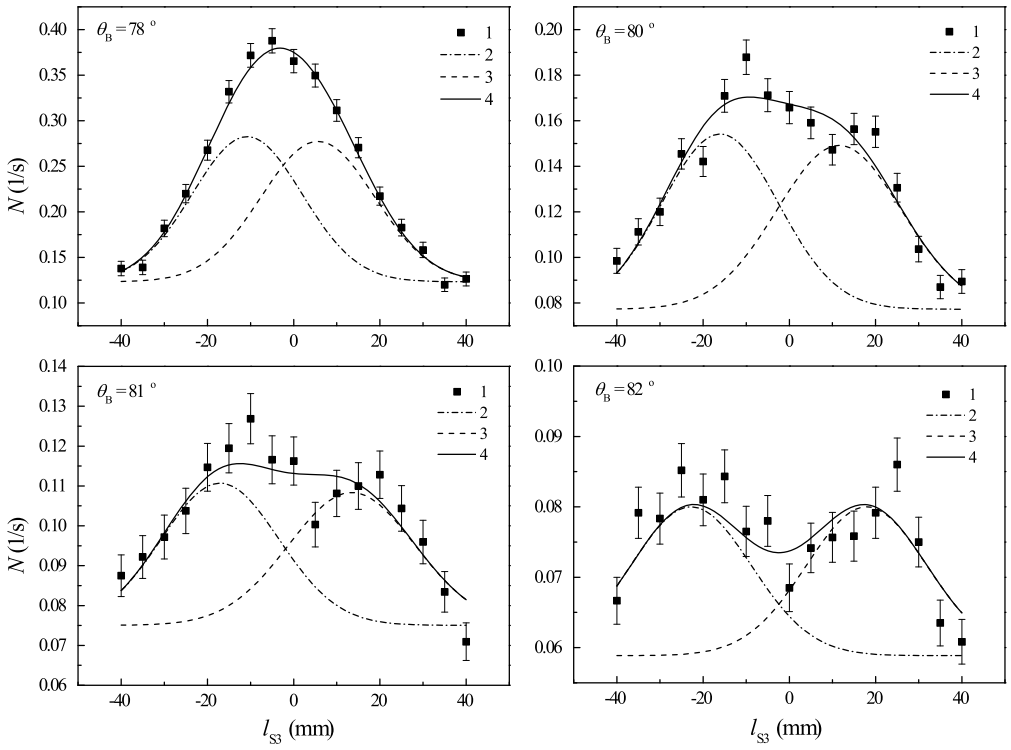

Fig. 4. Intensity distributions for different diffraction angles θ_B at the exit face of the crystal for a field gradient in the vicinity of the neutron beam. Filled squares with statistical error bars are the experimental data. The dotted curves denoted with (2) and (3) are fitted Gaussian profiles representing the reflexes of the two spin projections, and curve (4) is the sum of both (2) and (3).

a width of 1.6 mm. The entire silicon crystal is clamped onto a precision rotation stage, which itself is mounted onto translation stages (4). The precision goniometer is used to vary the Bragg angle θ_B and is controlled via an optical encoder with an precision of 0.03°. Everything is placed inside a thermostatic box consisting of an active and a passive thermal shield 7. The thermostat itself is connected to a temperature stabilized liquid circulator Julabo F34-HE, which allows to achieve a temperature stability of $\sim 0.01\,^{\circ}$C per day on the silicon crystal (under the conditions of the PF1b facility).

On the probing silicon crystal the neutron beam itself is collimated by two slits S_1, S_2 (see Fig. 2), while the spatial distribution on the exit of the probing crystal is scanned with slit S_3. The slit S_3 is mounted onto a piezomotor driven translation stage, which essentially eliminates all motion related heating of the crystal inside the thermostatic box. All slits are made from 0.5 mm thick cadmium metal.

Using permanent magnets and a special designed field guide (see Fig. 3) a field gradient is generated in the vicinity of the probing silicon crystal.

Opposing forces will act onto neutrons with opposite spin projection. Only force components perpendicular to the crystal planes along the reciprocal lattice vector **g** (y-axis) will contribute to a deviation from the Bragg condition:

$$F_y = \mp\mu \frac{\partial B}{\partial y}, \tag{14}$$

where $\partial B/\partial y$ – is the magnetic field gradient along y- axis, and μ – is the magnetic moment of the neutron.

After transmission through the crystal the diffracted neutrons are counted by the detector (8) (Fig. 2), which is protected from ambient background by the shielding (9). Neutrons not satisfying the conditions for diffraction are absorbed in the beam dump (10).

5. Results

The measurements were done for diffraction angles in the range of $\theta_B = 78° - 82°$. The minimum collimating slit openings of S_1=17 mm, S_2=15 mm, S_3=18 mm were chosen to optimize statistics during the given beam time.

The results of the measurement are shown in Fig. 4 and Fig. 5. In Fig. 4 the neutron intensity distribution at the exit of the probing crystal is shown as function of angle θ_B, where N denotes the measured intensity and l_{S3} is the position of the scanning slit S_3. The experimental data are shown as filled squares, while the curves denoted with (2) and (3) result from fitted Gaussian profiles representing the reflexes of the two spin projections and curve (4) is the sum of both.

Without a magnetic field the position of the intensity distribution coincides with that shown at $\theta_B = 78°$, but the width is slightly smaller and coincides with the widths of the dotted curves (2) and (3).

Since the primary neutron beam is unpolarized the two different spin projections are displaced with opposite sign. The difference in width and amplitude of the double-crystal lines (still having the same area under the curve) can be explained by the fact that one part is passing the crystal at larger distance (15 mm) with respect to the beam center. Due to the particular design of the field guide this is leading to an already substantial variation of the field gradient at these length scales.

In Fig. 5 we show the dependence of the splitting distance Δ_{exp} (filled circles) between the maxima of the double crystal reflexes for the two spin projections as function of the Bragg angle θ_B (see curves (2) and (3) in Fig. 4). From the plot it is evident that for a maximum diffraction angle of 82° the spatial splitting Δ_{exp} is 4.1 ± 0.1 cm.

From these data and using the equations (12) and (14) we can extract the value of the field gradient (open circles in Fig. 5)

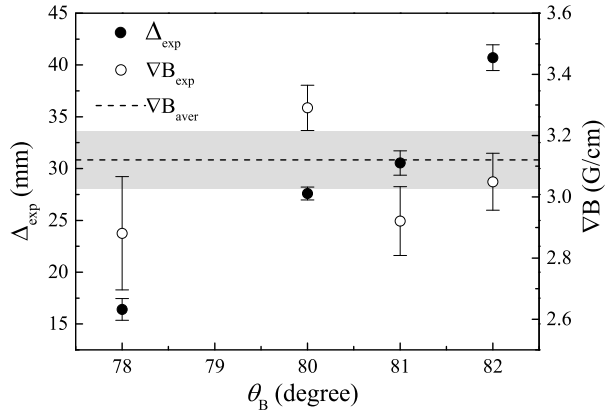

Fig. 5. Distance between the two intensity maxima of the two spin projections (see Fig. 4), field gradient as function of diffraction angle θ_B and calculated average value of the field gradient.

$$\frac{\partial B}{\partial y} = \frac{2E_n}{\mu K_e^{(220)} L^2} \cdot \frac{\Delta_{\exp}}{2}. \tag{15}$$

The average value of the field gradient along the neutron beam was calculated to be 3.12 ± 0.09 G/cm (see Fig. 5), which is consistent with estimates based on magnetometer readings at three points on each side (input and output) of the crystal 3.0 ± 0.3 G/cm. For comparison, the spatial split for neutrons with a wave length $\lambda = 3.8$ Å (which corresponds to Bragg angle of 82°) moving in free space under the same field gradient through the same 3-slit collimator without crystal (removed from the setup), can be calculated to be $3.9 \cdot 10^{-7}$ cm. From this we can deduce the measured diffractive amplification coefficient to be $K_{exp} \sim 2 \cdot 10^5 \tan^2 \theta_B$, which agrees well with theory.

Declaration of competing interest

The authors declare that they have no known competing financial interests or personal relationships that could have appeared to influence the work reported in this paper.

Acknowledgements

We are grateful to our colleagues V. Bellucci, R. Camattari and V. Guidi from Dipartimento di Fisica Universita di Ferrarà (Italy) for the support of this work. The reported study was funded by RFBR (19-32-90202).

References

[1] V.V. Voronin, V.V. Fedorov, I.A. Kuznetsov, et al., Phys. Proc. 17 (2011) 232.
[2] P.B. Hirsch, A. Howie, R.B. Nicholson, D.W. Pashley, M.J. Whelan (Eds.), Electron Microscopy of Thin Crystals, Plenum, New York, 1965.
[3] N. Kato, Acta Crystallogr. 13 (1960) 349.
[4] E.O. Vezhlev, V.V. Voronin, I.A. Kuznetsov, et al., JETP Lett. 96 (2012) 5.
[5] C.G. Shull, R. Nathans, Phys. Rev. Lett. 19 (1967) 384.
[6] M. Forte, J. Phys. G, Nucl. Phys. 9 (1983) 745.
[7] V.G. Baryshevskii, S.V. Cherepitsa, Phys. Status Solidi B 128 (1985) 379.
[8] V.L. Alekseev, E.G. Lapin, E.K. Leushkin, et al., J. Exp. Theor. Phys. 67 (1988) 1727.
[9] V.L. Alexeev, V.V. Fedorov, E.G. Lapin, et al., Nucl. Instrum. Methods Phys. Res., Sect. A 284 (1989) 181.
[10] J.M. Pendlebury, Nucl. Instrum. Methods Phys. Res., Sect. A 284 (1989) 227.
[11] V.V. Fedorov, V.V. Voronin, E.G. Lapin, J. Phys. G, Nucl. Part. Phys. 18 (1992) 1133.
[12] V.V. Fedorov, M. Jentschel, I.A. Kuznetsov, et al., Phys. Lett. B 694 (2010) 22.
[13] V.V. Fedorov, V.V. Voronin, Phys. At. Nucl. 77 (2014) 695.
[14] S.A. Werner, Phys. Rev. B 21 (1980) 1774.
[15] A. Zeilinger, C.G. Shull, M.A. Horne, et al., Phys. Rev. Lett. 57 (1986) 3089.
[16] B. Alefeld, G. Badurek, H. Rauch, Phys. Lett. A 83 (1981) 32.
[17] H. Weinfurter, G. Badurek, H. Rauch, et al., Z. Phys. B 72 (1988) 195.
[18] V.V. Voronin, Yu.V. Borisov, A.V. Ivanyuta, et al., JETP Lett. 96 (2012) 613.
[19] Y.P. Braginetz, Y.A. Berdnikov, V.V. Fedorov, et al., Phys. At. Nucl. 80 (2017) 38.
[20] C.G. Shull, Phys. Rev. Lett. 10 (1963) 297.
[21] T.R. Gentile, M.G. Huber, D.D. Koetke, et al., Phys. Rev. C 100 (2019) 034005.
[22] Yu.G. Abov, A.D. Gulko, P.A. Krupchitsky (Eds.), Polarized Slow Neutrons, Atomizdat, Moscow, 1966, in Russian.
[23] M. Forte, C.M.E. Zeyen, Nucl. Instrum. Methods Phys. Res., Sect. A 284 (1989) 147.
[24] V.V. Voronin, E.G. Lapin, S.Yu. Semenikhin, et al., JETP Lett. 72 (2000) 308.
[25] V.V. Voronin, V.V. Fedorov, S.Yu. Semenikhin, et al., J. Exp. Theor. Phys. 128 (2019) 347.
[26] V.V. Fedorov, A.I. Smirnov, J. Exp. Theor. Phys. 39 (1974) 271.
[27] C.G. Shull, A. Zeilinger, G.L. Squires, et al., Phys. Rev. Lett. 44 (1980) 1715.
[28] V.V. Voronin, E.G. Lapin, S.Yu. Semenikhin, et al., JETP Lett. 71 (2000) 76.
[29] E.O. Vezhlev, V.V. Voronin, I.A. Kuznetsov, et al., Phys. Part. Nucl. Lett. 10 (2013) 357.
[30] H. Abele, D. Dubbers, H. Häse, et al., Nucl. Instrum. Methods Phys. Res., Sect. A 562 (2006) 407.